Understanding the photoemission distribution of strongly interacting two-dimensional overlayers

Daniel Lüftner, ^{1,*} Simon Weiß, ^{2,3} Xiaosheng Yang, ^{2,3} Philipp Hurdax, ¹ Vitaliy Feyer, ⁴ Alexander Gottwald, ⁵ Georg Koller, ¹ Serguei Soubatch, ^{2,3,†} Peter Puschnig, ¹ Michael G. Ramsey, ¹ and F. Stefan Tautz^{2,3}

¹ Institut für Physik, Karl-Franzens-Universität Graz, NAWI Graz, Universitätsplatz 5, 8010 Graz, Austria

² Peter Grünberg Institut (PGI-3), Forschungszentrum Jülich, 52425 Jülich, Germany

³ Jülich Aachen Research Alliance (JARA), Fundamentals of Future Information Technology, 52425 Jülich, Germany

⁴ Peter Grünberg Institut (PGI-6), Forschungszentrum Jülich, 52425 Jülich, Germany

⁵ Physikalisch-Technische Bundesanstalt (PTB), Abbestraße 2-12, 10587 Berlin, Germany

(Received 5 May 2017; revised manuscript received 9 August 2017; published 5 September 2017)

Photoemission tomography (PT), the analysis of the photoemission intensity distribution within the plane wave final-state approximation, is being established as a useful tool for extracting the electronic and geometric structure of weakly interacting organic overlayers. Here we present a simple method for extending PT, which until now has been based on the calculations of isolated molecules. By including the substrate and a damped plane-wave final state, we are able to simulate the photoemission intensity distribution of two-dimensional molecular overlayers with both strong intermolecular and molecule-substrate interactions, here demonstrated for the model system 3,4,9,10-perylene-tetracarboxylic dianhydride (PTCDA) on Cu(100). It is shown that the interaction and hybridization of the lowest unoccupied molecular orbital of PTCDA with substrate states leads to its occupation and the formation of a strongly dispersing intermolecular band, whose experimental magnitude of 1.1 eV and k-space periodicity is well reproduced theoretically.

DOI: 10.1103/PhysRevB.96.125402

I. INTRODUCTION

The performance of organic-based devices depends on the geometric and electronic structure of the metal/organic interface, hence a detailed physical understanding of such interfaces is not only of fundamental interest, but it is also crucial to optimize the performance of actual devices [1–4], particularly in terms of an efficient charge transport. While bandlike transport is usually expected in organic single crystals along the direction of the π stacking [5–9], recently, several studies have shown evidence of significant intermolecular band dispersions in the lateral direction within well-ordered molecular monolayers [10-12]. The most direct experimental technique to study the electronic structure of metal-organic interfaces, in particular the occupied states, is angle-resolved photoemission spectroscopy (ARPES) [13]. However, a straightforward interpretation of the photoemission signal is not always easily possible and the help of theory becomes inevitable. In this context, density functional theory (DFT) has become the standard tool to study the electronic structure of the interface, but due to the limitations of Kohn-Sham (KS) DFT, a one-to-one comparison of the KS eigenvalues to results from ARPES measurements may lead to an erroneous assignment of individual molecular orbitals to the peaks in the photoemission spectrum [14–17]. Fortunately, in recent years a technique called photoemission tomography (PT) has emerged [18,19]. In PT scans through ARPES, patterns of well-ordered molecular monolayers on metallic substrates are compared to the Fourier transform of the orbitals of an isolated molecule [20]. The approximation of the final state by a plane wave allows one not only to deconvolute the photoemission spectra and unambiguously assign individual

orbitals of the adsorbed molecules to specific peaks in the recorded spectrum [12,16,19,21–24] but also to determine the molecular orientation [25] or the occupied orbital orientation after degeneracy breaking [26], to assign specific vibronic modes [27] or even to obtain real space images of molecular orbitals [28–30]. While for weakly interacting systems, like those cited above, a treatment in terms of isolated molecules has been justified, it is not expected to be applicable to systems with strong substrate and/or intermolecular interactions.

The aim of this work is to extend the PT approach to two-dimensional overlayers that exhibit strong intermolecular and molecule-substrate interactions. This is achieved in two steps, first, by the modification of the initial state of the photoemission process, as we no longer restrict ourselves to orbitals of an isolated molecule but rather use the Bloch states of periodic systems including the substrate. The inclusion of the substrate requires the second step in the extension of the PT approach, because the simple plane wave leads to an overestimation of the contributions of bulk substrate states. To overcome this, we modify the final state by exponentially damping the plane wave into the substrate, thus mimicking the mean-free-path length of photoemitted electrons in a bulk material [31].

With both strong molecule-substrate interactions [32] as well as significant intermolecular interactions in the two-dimensional (2D) overlayer structure, the interface of 3,4,9,10-perylene-tetracarboxylic dianhydride (PTCDA) on Cu(100) has turned out to be an ideal test system for our extended PT approach, enabling a relatively complete understanding of the complex photoemission intensity distribution. Following the two-step strategy outlined above, we first calculate the structure and electronic states at the PTCDA/Cu(100) interface using DFT with an appropriate van-der-Waals correction. Then we apply the calculated electronic structure including molecular and substrate contributions to simulate the photoe-

^{*}daniel.lueftner@uni-graz.at

[†]s.subach@fz-juelich.de

mission fingerprints of those states in reciprocal space, using a damped plane-wave final state. We find that the hybridization of the lowest unoccupied molecular orbital (LUMO) of PTCDA leads to its occupation and the formation of a highly dispersing intermolecular band, whose experimental magnitude and character are well reproduced by the theoretical approach suggested in this paper.

II. EXPERIMENTAL DETAILS

Ordered monolayers of PTCDA on Cu(100) were prepared by thermal sublimation of PTCDA in vacuum and deposition onto the Cu(100) surface. Prior to deposition, the Cu(100) surface was cleaned by several cycles of annealing at 500°C and sputtering by Ar ions. The expected structure of the PTCDA monolayer on Cu(100) was validated by low-energy electron diffraction, carried out before the photoemission experiments.

Angle-resolved photoemission experiments were conducted using both the photoemission electron microscope (PEEM) from Omicron NanoTechnology GmbH at the NanoESCA beamline [33] of the Elettra Sincrotrone (Trieste, Italy) and a toroidal electron-energy analyzer [34] at the Metrology Light Source [35] of the Physikalisch-Technische Bundesanstalt (Berlin, Germany), with compatible results in both cases. The experiments were performed at room temperature with p-polarized light at angles of incidences of 65° and 40° to the surface normal, respectively. The PEEM allows the collection of all emissions in a cone with a maximum radius in reciprocal space of about 2 Å⁻¹. In the toroidal analyzer all emissions in the plane of incidence from -85.5° to $+85.5^{\circ}$ are collected. For the photon energy of 31 eV which we employed, this allows k values up to 2.5 Å^{-1} to be detected, with the momentum maps obtained by rotating the crystal azimuth in 1° steps.

III. COMPUTATIONAL DETAILS

Our theoretical photoemission simulations are based on results obtained within the framework of DFT. We have performed two types of calculations: first, for the isolated PTCDA molecule, which was performed by utilizing the DFT code ABINIT [36] and, second, for the full PTCDA/Cu(100) overlayer, for which the VASP code [37,38] was used.

The calculations of the isolated molecule employ a supercell approach with a vacuum of at least ≈15 Å between different PTCDA molecules in each direction. We use the generalized gradient approximation (GGA) [39] for exchange-correlation effects. The simulated momentum maps of the highest occupied molecular orbital (HOMO) and the LUMO of the isolated PTCDA molecule are obtained as Fourier transforms of the respective Kohn-Sham orbital as described below.

The electronic structure calculations for PTCDA monolayers adsorbed on Cu(100) use a repeated slab approach. The metallic substrate is modeled by five metallic layers and a vacuum layer of ≈ 15 Å has been added between the slabs. To avoid spurious electrical fields, a dipole layer is inserted in the vacuum region [40]. The GGA [39] is used for exchange-correlation effects, and the projector augmented

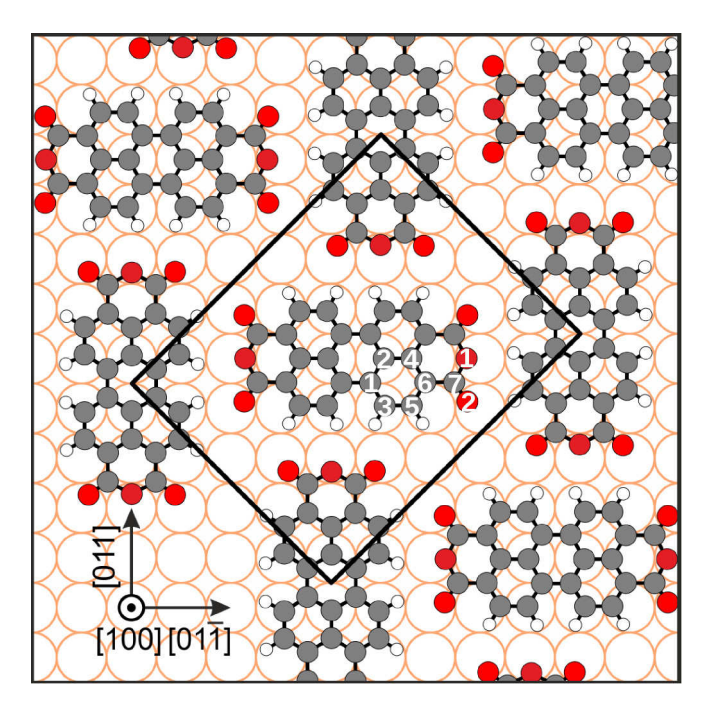


FIG. 1. Structural model of the PTCDA/Cu(100) overlayer (from Refs. [32,44]). The white numbers label the inequivalent carbon and oxygen atoms.

wave (PAW) [41] approach is used, allowing for a relatively low-kinetic-energy cutoff of $500 \, \text{eV}$. We use a Monkhorst-Pack $7 \times 7 \times 1$ grid of k points [42] and a first-order Methfessel-Paxton smearing of $0.1 \, \text{eV}$ [43]. The supercell geometry is constructed according to the experimental LEED structure [44]. During geometry optimization, the atomic positions of the molecular layer and the first two metallic layers are allowed to relax. In order to account for van der Waals interactions, we employ the vdW-surf method according to Ruiz *et al.* [45,46] in the geometry optimization.

Of the two proposed adsorption sites [44] with the PTCDA molecule centered at the Cu-Cu bridge site and its long molecular axis either on top or between the atomic rows of the Cu substrate, we found that the former is energetically more favorable by about 0.75 eV per molecule. A schematic image of the so-obtained interface geometry is depicted in Fig. 1. A similar conclusion regarding the adsorption site was recently reached from normal incidence x-ray standing wave triangulation analysis [32]. Moreover, unlike on Ag surfaces [47], the calculations reveal that the backbone of the PTCDA molecule is located closer to the Cu substrate than its ends, with the anhydride (O1) and carboxylic (O2) oxygen atoms and the functional carbon atoms (C7) bending away from the surface in agreement with experiment [32], as can be seen by the distances of the individual atoms from the surface given in Table I. Hence, both the calculated adsorption site and adsorption height are in excellent agreement with experiment [32].

The density of states (DOS) ρ_i projected onto molecular orbital i is calculated as the overlap of the Bloch function $\phi_{i\mathbf{q}}$ of the corresponding orbital i calculated for a freestanding PTCDA film with the Bloch states $\psi_{n\mathbf{q}}$ and the corresponding

TABLE I. Calculated adsorption heights of PTCDA's carbon and oxygen atoms on Cu(100). The numbering of the individual atoms is shown in Fig. 1.

energies $\varepsilon_{n\mathbf{q}}$ of the full PTCDA/Cu(100) system via

$$\rho_i(E) = \sum_{\mathbf{q}} \sum_{n} |\langle \phi_{i\mathbf{q}} | \psi_{n\mathbf{q}} \rangle|^2 \delta(E - \varepsilon_{n\mathbf{q}}). \tag{1}$$

Here n is the band index and \mathbf{q} the wave vector in the first Brillouin zone.

IV. PHOTOEMISSION INTENSITIES

The calculated electronic states were used to approximate the quasiparticle energies and wave functions in the modified PT approach. In particular, the Kohn-Sham eigenvalues $\varepsilon_{n\mathbf{q}}$ and eigenstates $\psi_{n\mathbf{q}}$, respectively, are utilized as input for the computation of photoemission intensity patterns. In our approach, the photoemission process is treated perturbatively and within the one-step model of photoemission. Furthermore, we use the independent particle picture in which the spectral function is replaced by the δ function, thus ensuring energy conservation. The intensity I is then given by a Fermi's Golden rule expression [48,49]

$$I \propto \sum_{n}^{\text{occ}} \sum_{\mathbf{q}}^{\text{BZ}} |\langle \psi_f | \mathbf{A} \cdot \mathbf{p} | \psi_{n\mathbf{q}} \rangle|^2 \times \delta(\varepsilon_{n\mathbf{q}} + \Phi + E_{\text{kin}} - h\nu).$$
(2)

Here $h\nu$ is the energy of the incoming photon, $E_{\rm kin}$ is the kinetic energy of the emitted electron, and Φ is the work function of the system under study. The interaction operator for the transition between the initial states $\psi_{n{\bf q}}$ and the final state ψ_f includes the vector potential ${\bf A}$ of the incoming photon and the momentum operator ${\bf p}$ of the electron [50].

In general, the summation in Eq. (2) runs over all occupied initial states and all $\bf q$ points sampling the first Brillouin zone. However, if a qualitative agreement between the measured and the calculated photoemission intensity map is sufficient, which is the case for many applications of PT [19–21,24–26,51], then the simulated momentum map may be obtained from a single molecular orbital of an isolated molecule where only the Γ point has to be taken into account. In this case, the double sum in Eq. (2) can be omitted and the single molecular orbital ϕ_i of an isolated molecule is used as initial state, yielding

$$I(k_x, k_y; h\nu, \mathbf{A}) \propto |\langle \psi_f | \mathbf{A} \cdot \mathbf{p} | \phi_i \rangle|^2 \times \delta(E_i + \Phi + E_{\text{kin}} - h\nu).$$
(3)

With this simplified approach, however, the influence of intermolecular and molecule-substrate interactions on the momentum maps cannot be taken into account. If these interactions become significant, then the full interface [here

PTCDA/Cu(100)] has to be considered, and the Bloch states $\psi_{n\mathbf{q}}$ together with an appropriate sampling of the Brillouin zone have to be taken as initial state.

The choice of the final state ψ_f of the photoemission process is crucial when evaluating Eq. (2) [52]. The simplest approximation for the final state is a plane wave [20,53]. With that assumption, the matrix element in Eq. (2) greatly simplifies, and its evaluation reduces to a Fourier transform of the initial state $\psi_{n\mathbf{q}}$ modulated by an angle-dependent geometry factor $|\mathbf{A} \cdot \mathbf{k}|^2$ [20],

$$I(k_x, k_y; h\nu, \mathbf{A}) \propto \sum_{n}^{\text{occ}} \sum_{\mathbf{q}}^{\text{BZ}} |\mathbf{A} \cdot \mathbf{k}|^2 |\langle e^{i\mathbf{k}\mathbf{r}} | \psi_{n\mathbf{q}} \rangle|^2$$
$$\times \delta(\varepsilon_{n\mathbf{q}} + \Phi + E_{\text{kin}} - h\nu), \tag{4}$$

where **k** corresponds to the momentum of the outgoing electron. For the full interface, the initial state, i.e., the Kohn-Sham eigenfunctions of the DFT calculations, are represented using a plane-wave basis set and the Bloch states $|\psi_{n\mathbf{q}}\rangle$ are, apart from a normalization factor, given by

$$|\psi_{n\mathbf{q}}\rangle = \sum_{\mathbf{G}}^{|\mathbf{G}| < G_{\text{cut}}} c_{n\mathbf{q}}(\mathbf{G}) e^{i(\mathbf{q} + \mathbf{G})\mathbf{r}}.$$
 (5)

Here **G** are reciprocal lattice vectors and the sum in Eq. (5) runs over all reciprocal lattice vectors below the given energy cutoff. The transition matrix element $\langle e^{i\mathbf{k}\mathbf{r}}|\psi_{n\mathbf{q}}\rangle$ of Eq. (4) is for this case the sum of those plane wave coefficients whose reciprocal lattice vector **G** equals the difference between the final-state momentum **k** and the momentum **q** of the initial Bloch state and hence is given by

$$\langle \psi_{n\mathbf{q}} | e^{i\mathbf{k}\mathbf{r}} \rangle = \sum_{\mathbf{G}} c_{n\mathbf{q}}^*(\mathbf{G}) \delta_{\mathbf{G},\mathbf{k}-\mathbf{q}}.$$
 (6)

While for isolated molecules, the plane-wave final state has been shown to give good agreement with experiment [20,28], it is problematic when the substrate is included in the calculations. This is because the plane-wave final state overestimates the photoemission signal of the substrate states, because the limited mean-free-path length of the photoemitted electrons is not taken into account. To mimic the escape length of the photoelectrons, we therefore modify the final-state plane wave by an exponential damping inside the crystal [54]. This damped plane wave is defined in an empirical form using two parameters, z_0 and γ . For the evaluation of Eq. (2), the unit cell is divided into two regions in the z direction, i.e., the direction of the surface normal. The region above the substrate $(z > z_0)$ is treated by a pure plane wave, while below z_0 the plane wave is exponentially damped with the parameter γ in the exponent, whose inverse $\frac{1}{\nu}$ represents the mean free path. Thus, the final state is given by

$$|\psi_f\rangle = \begin{cases} e^{i\mathbf{k}\mathbf{r}} e^{\gamma(z-z_0)} & z < z_0\\ e^{i\mathbf{k}\mathbf{r}} & z \geqslant z_0. \end{cases}$$
 (7)

A schematic view of the damped final state in the direction normal to the surface is shown in Fig. 2. To compute the photoemission intensities with this damped final state, $|\psi_f\rangle$ is inserted into Eq. (2) and the matrix elements are evaluated for all Bloch bands $\psi_{n\mathbf{q}}$ at each reciprocal lattice point \mathbf{q} . For the

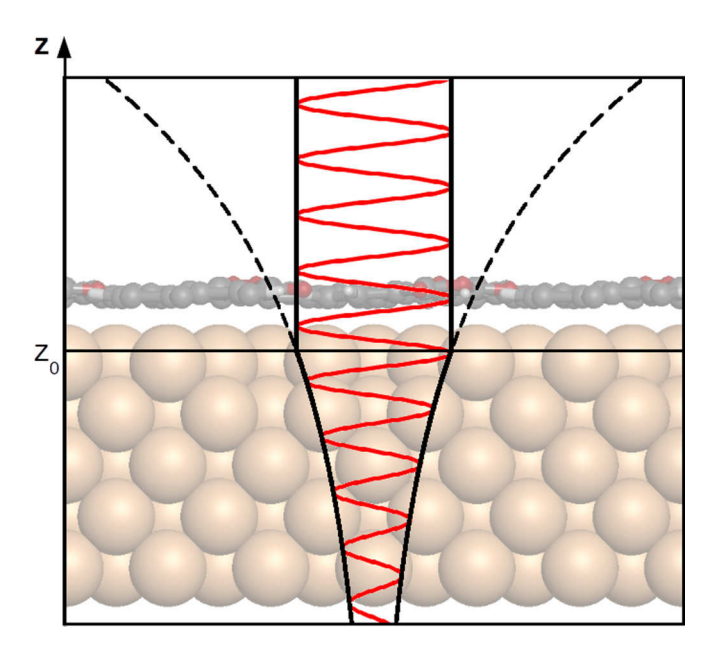


FIG. 2. Schematic sketch of the final state used in our calculation of photoemission intensities. The final state is a plane wave that is damped in the z direction of the unit cell. Above z_0 the final state is treated as a pure plane wave, and below z_0 it is exponentially damped by the factor $e^{\gamma(z-z_0)}$, which is shown as the black envelope of the damped plane wave.

case of a damped plane wave, the evaluation of the transition matrix element leads to the following expression:

$$\langle \psi_{n\mathbf{q}} | \mathbf{A} \cdot \mathbf{p} | \psi_f \rangle_d = (i\mathbf{A}\mathbf{k} + A_z \gamma) \sum_{\mathbf{G}} c_{n\mathbf{q}}^*(\mathbf{G}) \delta_{G_x, k_x - q_x} \delta_{G_y, k_y - q_y}$$

$$\times \left(\frac{e^{-ig_z z_0} - e^{\gamma z_0}}{-ig_z + \gamma} - \frac{e^{-ig_z c} - e^{-ig_z z_0}}{-ig_z} \right). \tag{8}$$

Here we have abbreviated the z component of the vector $\mathbf{g} = \mathbf{G} + \mathbf{q} - \mathbf{k}$ as g_z and introduced the lattice constant c of the supercell of the full interface in the z direction.

In order to account for the intrinsic energy resolution in the photoemission experiment, the δ function is replaced by a Gaussian distribution in the numeric evaluation of Eq. (2). In this work, the width of the Gaussian is chosen as 0.1 eV, similar to the experimental energy resolution. In addition, due to finite resolution of the k mesh that samples the first Brillouin zone, also the Kronecker δs in Eqs. (6) and (8) are replaced by a Gaussian function. These replacements prevent spurious modifications of the photoemission pattern due to a too-coarse k mesh used in the DFT calculation. The width of the distribution has been chosen as small as possible such that no spurious substructures are seen in the simulated patterns. That is usually achieved when the width is chosen slightly larger than the distance between the k points that sample the first Brillouin zone. In the case of a $7 \times 7 \times 1$ grid of k points the width has been chosen as 0.05 Å^{-1} .

Note that even with the damped plane wave, the description of the photoemission process remains a simple one. As

such, it is not designed for a correct description of the photoemission intensities of the substrate but rather allows us to describe the influence of intermolecular and moleculesubstrate interactions onto the emission patterns. Furthermore, important insights may be obtained when the results of both the plane-wave [Fig. 3(a), according to Eq. (4)] and dampedplane-wave final-state calculations [Fig. 3(b), according to Eq. (8)] are compared. Thereby, the emission contributions from adsorbate and substrate states can be clearly distinguished in the simulated pattern. Figure 3(c) shows the differential photoemission intensity map computed as $(I_{\rm pw}-I_{\rm dpw})/I_{\rm dpw},$ where I_{pw} and I_{dpw} are the photoemission intensities calculated within the pure plane-wave approximation [Fig. 3(a)] and using the damped plane wave [Fig. 3(b)], correspondingly. Thus, the red highlights emissions that originate in the substrate, because the intensity of these states is significantly suppressed when a damped plane wave is used, while the contributions from molecular states stay the same. The difference can be seen best in the energy range of the Cu d bands between approximately -2.5 and $-4\,\mathrm{eV}$ and in the parabolic feature starting from Γ at a binding energy of about $-1.5\,\mathrm{eV}$, both of which are revealed to be substrate features. Furthermore, as can be seen at the blue region in Fig. 3(c) at about -1.7 Å^{-1} , the drop of intensity to zero when $\mathbf{A} \perp \mathbf{k}$ that is present for the plane-wave final state vanishes for the damped plane wave due to a second contribution in the polarization factor proportional to the damping parameter γ [see Eq. (8)] [54].

V. RESULTS AND DISCUSSION

We now turn to the results of the angular-resolved photoemission experiments on the ordered PTCDA monolayer on Cu(100). Energy distribution curves of the photoemission [Fig. 4(a)] reveal two molecular emissions at $-1.7 \, \text{eV}$ and $-0.8\,\mathrm{eV}$ in the vicinity of the Fermi level whose relative intensities strongly depend on the azimuthal angle of emission. In order to identify the origin of these emissions, momentum maps at corresponding binding energies [Figs. 4(b) and 4(c)] have been recorded and compared to those calculated for the KS orbitals of two perpendicular oriented molecules [Figs. 4(e) and 4(f)], as suggested by the known overlayer structure of a PTCDA monolayer on Cu(100) [32,44,55] (Fig. 1). The simulated momentum maps of the PTCDA highest occupied and lowest unoccupied molecular orbitals (HOMO and LUMO) resemble the experimental ones measured at binding energies (BE) of $-1.7 \,\text{eV}$ and $-0.8 \,\text{eV}$, respectively. Therefore, these emissions are assigned to the PTCDA HOMO and LUMO. The latter orbital is populated due to electron donation from the substrate [21,56]. Apart from a 0.4 eV energy shift of the HOMO between experiment and theory, this assignment is also in accordance with the calculated density of states of the adsorbed monolayer on Cu(100) projected onto the LUMO and HOMO of the molecule depicted in Fig. 4(d).

Closer inspection of the experimental momentum map of the LUMO [Fig. 4(c)] reveals a substructure within the principal emission lobes that is not present in the calculations using only the isolated molecule [Fig. 4(f)]. In order to investigate its origin, we have recorded energy band maps

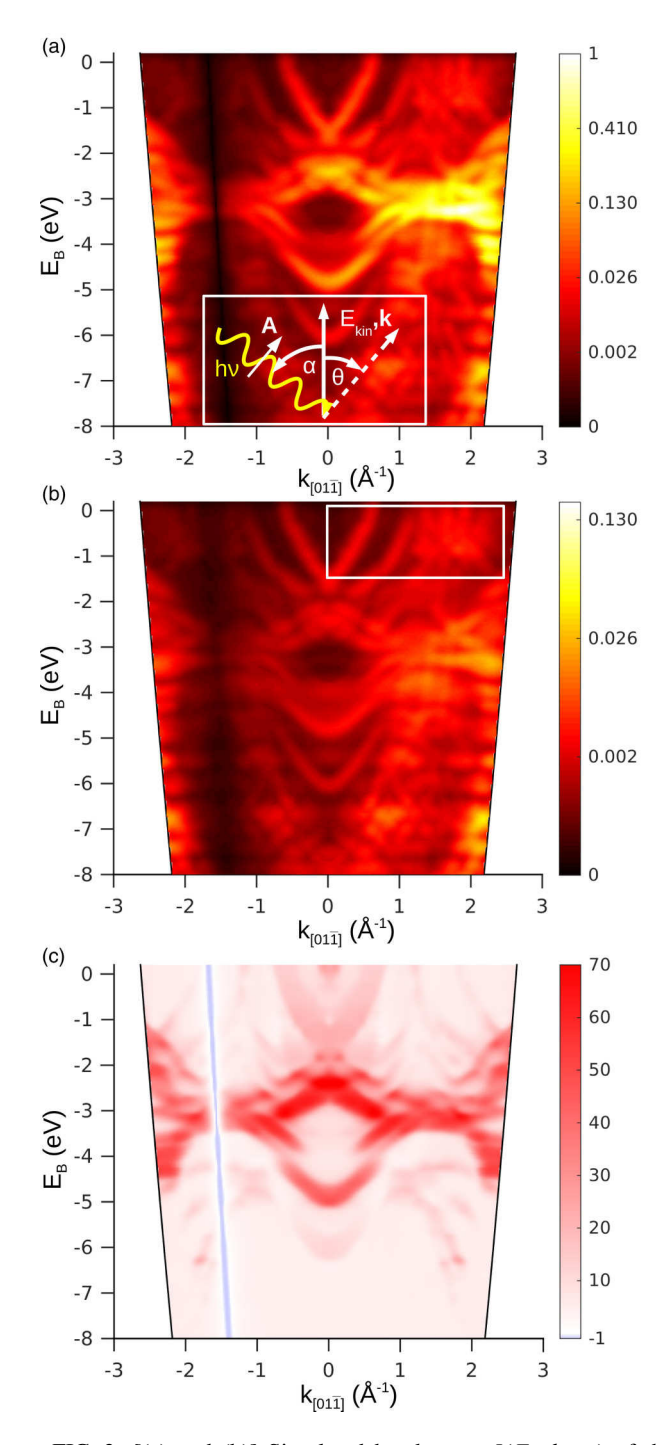


FIG. 3. [(a) and (b)] Simulated band maps $I(E_B, k_{[01\bar{1}]})$ of the PTCDA/Cu(100) interface, using a pure plane wave (a) and a damped plane wave (b) with the damping parameter $\gamma=0.25\,\text{Å}^{-1}$ for the final state, respectively. The insert in panel (a) shows a schematic of the experimental geometry, defining the angle of incidence α , the corresponding polarization vector **A**, and the momentum vector **k** for a given emission angle θ . The white box in panel (b) indicates the energy and wave vector range which is considered in more detail in Fig. 5. A photon energy of 31 eV and an angle of incidence of 40° has been utilized in the simulation of the band map. (c) Differential photoemission intensity band map computed as $(I_{\rm pw}-I_{\rm dpw})/I_{\rm dpw}$, where $I_{\rm pw}$ and $I_{\rm dpw}$ are the photoemission intensities calculated within pure plane-wave approximation and using the damped plane wave, respectively.

 $I(E_B,k_{\parallel})$, as well as a series of constant BE momentum maps, in an energy and wave vector range indicated by the white box in Fig. 3(b). Looking at the energy band map [Fig. 5(a)] we immediately find that the LUMO intensity oscillates in the k region between 1.4 and 2.1 Å^{-1} over an energy range of about 1.1 eV. The period of the oscillation is about 0.27 Å^{-1} . which can be seen best at the low binding energy side of the bright feature in Fig. 5(a), where four maxima can be identified. This period of the oscillation transforms to a real space distance of about 23.3 Å, which is close to the diagonal of the PTCDA/Cu(100) unit cell (23.11 Å). Despite these modifications of its principal emission lobes, present in both principal azimuths, the character of the LUMO is preserved over its entire energy range. This can be seen when looking at experimental momentum maps recorded at different binding energies shown in the left halves of Figs. 5(d)-5(f), where all three maps carry the major shape of the LUMO pattern. Interpreting all the findings, we conclude that the modifications in the shape of the LUMO photoemission pattern have their origin in a surprisingly large intermolecular band dispersion of the former LUMO.

To support this hypothesis, we have performed DFT calculations for two model systems: the PTCDA/Cu(100) monolayer and the freestanding monolayer of PTCDA with the same molecular arrangement. In the computed band map of the freestanding layer, the LUMO-derived band shows a dispersion of only 20 meV, two orders of magnitude lower than observed in the experiment. Figure 5(c) shows the band map of the freestanding layer as it would appear with an experimental resolution of 100 meV.

If we include the substrate in the DFT calculation and apply the damped plane-wave approach, then the resulting band map [Fig. 5(b)] displays an oscillating, dispersive substructure in the region of the LUMO. Both the periodicity and the band width, highlighted by the dotted line as a guide for the eye, are in excellent agreement with the experimental band map [Fig. 5(a)]. When considering the difference band map in Fig. 3(c), it becomes apparent that this feature is of molecular origin, as the plane wave and damped plane wave give about the same intensity, and significant substrate-enhanced intermolecular dispersion is concluded.

As the experiment [left halves of Figs. 5(d)-5(f)], the calculation, displayed in the right halves of Figs. 5(d)-5(f), also shows that the character of the LUMO is preserved over the whole energy range of dispersion: The LUMO pattern can be clearly recognized at the top, middle, and bottom of the band. In addition, the experimentally observed substructure in the LUMO's main lobe is reproduced in the calculation, suggesting the substructure to be due to intermolecular dispersion. The simulation also shows the increase of the LUMO's band width by two orders of magnitude when going from a freestanding to the adsorbed monolayer. Thus the observed photoemission intensity pattern can be understood as that of an isolated molecule modified by intermolecular band dispersion that has been strongly enhanced by moleculesubstrate interactions. These strong interactions, which lead to a hybridization of molecule and substrate states, correlate with the small adsorption height of the molecule, with the C backbone closest to the Cu(100) surface. The observed large

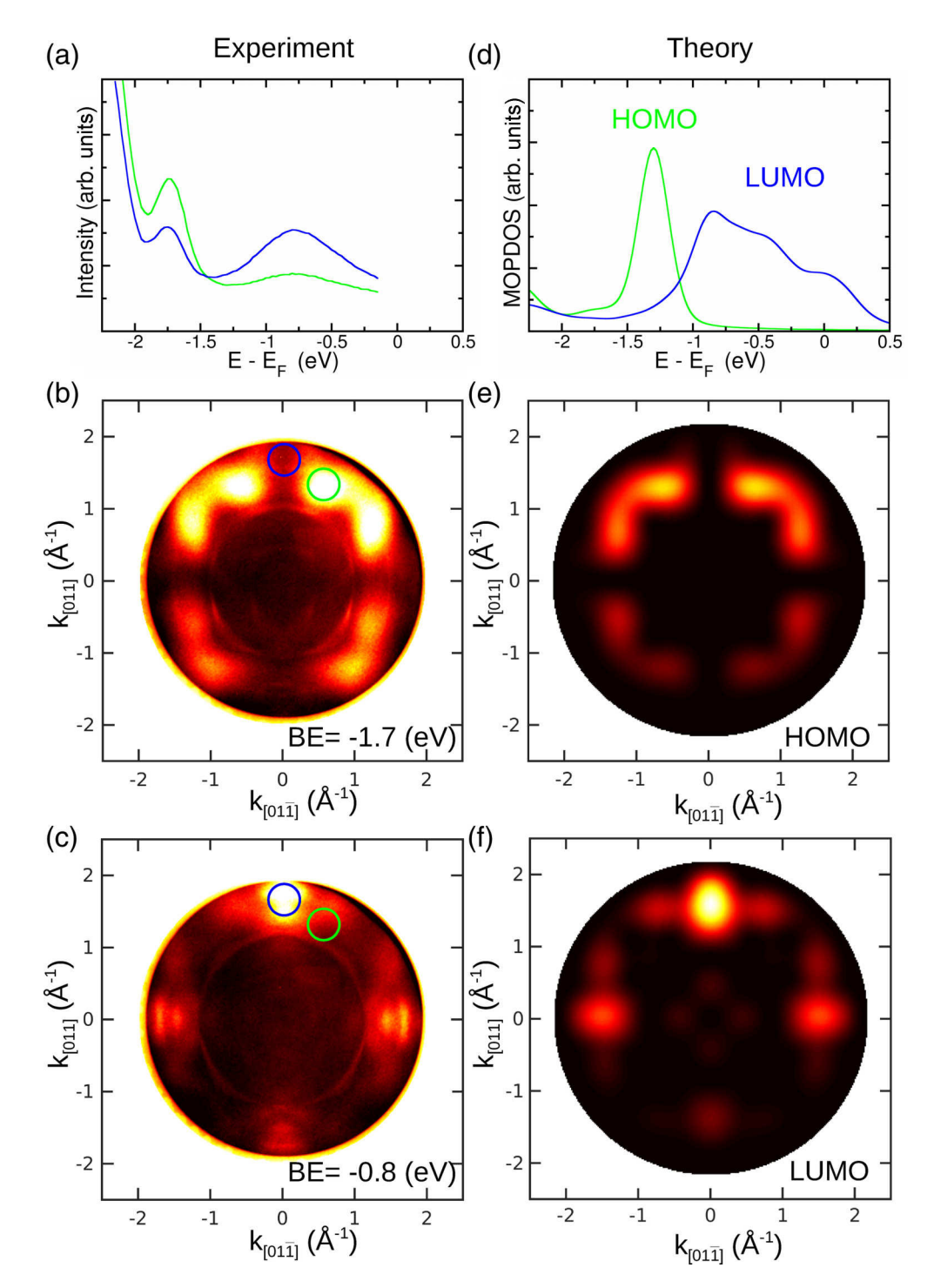


FIG. 4. (a) Photoemission spectra measured in the k region indicated by the blue and green cricles in panels (b) and (c). (d) Calculated density of states for the PTCDA/Cu(100) heterostructure, projected onto the HOMO and LUMO of PTCDA. [(b) and (c)] Measured momentum maps at the peak energies of $-1.7 \,\text{eV}$ and $-0.8 \,\text{eV}$, respectively. [(e) and (f)] Simulated momentum maps for the HOMO and LUMO of isolated PTCDA, respectively. A photon energy of 35 eV and angle of incidence of 65° in the plane of incidence containing the [011] direction were used in both the PEEM experiment and the simulation.

band width (1.1 eV) in combination with a small k periodicity (0.27 Å⁻¹) implies a low effective mass of only 0.02 m_e when assuming a cosinelike dispersion.

Intermolecular dispersion in monolayers has been observed for other systems [10-12]. In the work of Wießner *et al.*

[10,11], the calculated band width of freestanding and adsorbed monolayer are of the same magnitude, suggesting only a minor enhancement of the intermolecular dispersion by the substrate. Note that the dispersion of the molecular states measured by Wießner *et al.* becomes visible only by a specific

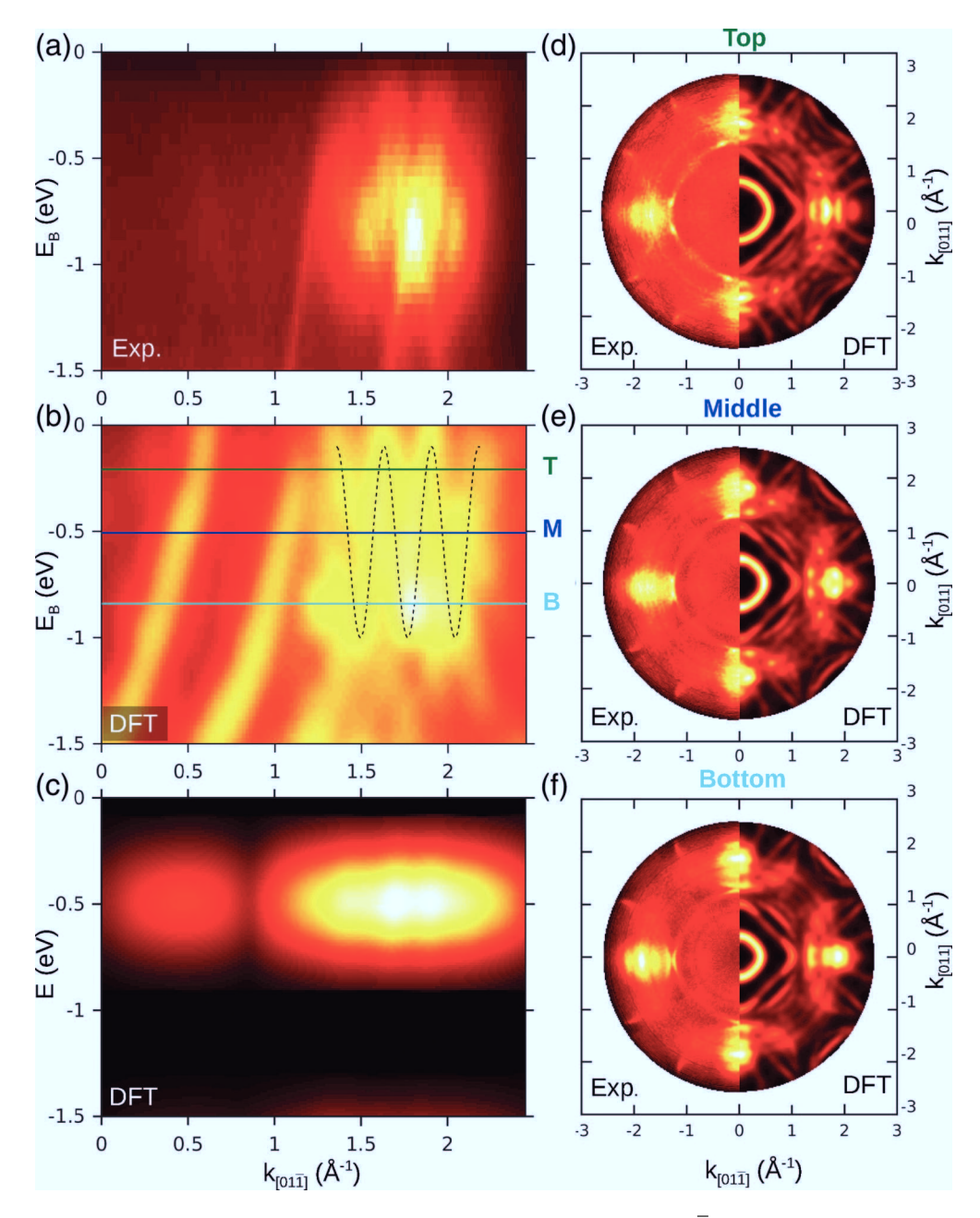


FIG. 5. (a) Measured band map $I(E_B, k_{[01\bar{1}]})$, along the principal azimuth in the $[01\bar{1}]$ direction. (b) Simulated band map of the PTCDA/Cu(100) heterostructure. The dotted line is merely a guide to the eye. (c) Simulated band map of the freestanding PTCDA layer, with the LUMO centered at the same energy as for the case of PTCDA/Cu(100) heterostructure. [(d)-(f)] Experimental (left halves) and simulated (right halves) momentum maps $I(k_{[01\bar{1}]},k_{[011]})$ at the top, middle, and bottom of the band, as indicated by the horizontal lines in panel (b). A photon energy of 31 eV and an angle of incidence of 40° has been used in both the toroidal analyzer experiment and the simulation.

normalisation of the photoemission intensities between the Γ point and the molecular feature. Similarly to our results, Ules *et al.* [12] directly detected the dispersion of the LUMO of pentacene on the Cu(110) surface, manifesting itself in a modification of the momentum pattern of an isolated molecule. However, because of the incommensurable overlayer structure of pentacene on Cu(110), these modifications could only be explained heuristically on the basis of the periodicity of the adsorbed monolayer, as the molecule-substrate system could not be calculated. While the characteristic modification

of the momentum maps over the dispersing band could be reproduced, its bandwidth could not be directly calculated and compared quantitatively to experiment and the substrate-enhanced dispersion had to be invoked [12].

VI. CONCLUSION

In conclusion, we have presented a method to simulate the photoemission intensity distribution of two-dimensional molecular overlayers that exhibit strong intermolecular and molecule-substrate interactions. We show that the initial state of the photoemission process can be approximated by the Bloch states of the entire calculated overlayer-substrate system and the final state by a damped plane wave. A comparison to simulations using a simple plane wave allows us to disentangle the contributions of substrate and molecular adsorbate states to the photoemission intensity. Furthermore, we demonstrate that the method allows the characterization of the electronic structure of an organic/metallic interface beyond a simple assignment of photoemission peaks to particular molecular orbitals in the photoemission spectrum. Specifically, we are able to reproduce the observed strong intermolecular dispersion of the molecule's LUMO, which is enhanced by two orders of magnitude through substrate interactions, in terms of

both its momentum map pattern and its bandwidth. As such, our approach extends the PT technique to strongly interacting systems allowing their rather complex photoemission intensity distribution to be simply understood.

ACKNOWLEDGMENTS

We thank T. Ules, B. Stadtmüller, T. Sueyoshi, and D. Schwarz for experimental support. We also want to thank H. Kaser and M. Richter for the support at the Metrology Light Source. We acknowledge financial support from the Austrian Science Fund (FWF) Projects No. P27649-N20 and No. P27427-N20. The computational results presented have been achieved using the computing facilities of the University of Graz and the Vienna Scientific Cluster (VSC3).

- A. Kahn, N. Koch, and W. Gao, J. Polym. Sci., Part B: Polym. Phys. 41, 2529 (2003).
- [2] F. S. Tautz, Prog. Surf. Sci. 82, 479 (2007).
- [3] N. Koch, Chem. Phys. Chem. 8, 1438 (2007).
- [4] Edited by N. Koch, N. Ueno, and A. T. S. Wee, *The Molecule-Metal Interface* (Wiley-VCH, Weinheim, 2013).
- [5] N. Koch, A. Vollmer, I. Salzmann, B. Nickel, H. Weiss, and J. P. Rabe, Phys. Rev. Lett. 96, 156803 (2006).
- [6] G. Koller, S. Berkebile, M. Oehzelt, P. Puschnig, C. Ambrosch-Draxl, F. P. Netzer, and M. G. Ramsey, Science 317, 351 (2007).
- [7] N. Ueno and S. Kera, Prog. Surf. Sci. 83, 490 (2008).
- [8] S. Berkebile, P. Puschnig, G. Koller, M. Oehzelt, F. P. Netzer, C. Ambrosch-Draxl, and M. G. Ramsey, Phys. Rev. B 77, 115312 (2008).
- [9] F. Ortmann, F. Bechstedt, and K. Hannewald, Phys. Status Solidi B 248, 511 (2011).
- [10] M. Wießner, J. Ziroff, F. Forster, M. Arita, K. Shimada, P. Puschnig, A. Schöll, and F. Reinert, Nat. Commun. 4, 1514 (2013).
- [11] M. Wießner, J. Kübert, V. Feyer, P. Puschnig, A. Schöll, and F. Reinert, Phys. Rev. B 88, 075437 (2013).
- [12] T. Ules, D. Lüftner, E. M. Reinisch, G. Koller, P. Puschnig, and M. G. Ramsey, Phys. Rev. B 90, 155430 (2014).
- [13] S. Hüfner, *Photoelectron Spectroscopy* (Springer, Berlin, 2003).
- [14] S. Kümmel and L. Kronik, Rev. Mod. Phys. 80, 3 (2008).
- [15] T. Körzdörfer, S. Kümmel, N. Marom, and L. Kronik, Phys. Rev. B 79, 201205(R) (2009).
- [16] M. Dauth, T. Körzdörfer, S. Kümmel, J. Ziroff, M. Wiessner, A. Schöll, F. Reinert, M. Arita, and K. Shimada, Phys. Rev. Lett. 107, 193002 (2011).
- [17] D. Lüftner, S. Refaely-Abramson, M. Pachler, R. Resel, M. G. Ramsey, L. Kronik, and P. Puschnig, Phys. Rev. B 90, 075204 (2014).
- [18] J. Ziroff, F. Forster, A. Schöll, P. Puschnig, and F. Reinert, Phys. Rev. Lett. 104, 233004 (2010).
- [19] P. Puschnig, E.-M. Reinisch, T. Ules, G. Koller, S. Soubatch, M. Ostler, L. Romaner, F. S. Tautz, C. Ambrosch-Draxl, and M. G. Ramsey, Phys. Rev. B 84, 235427 (2011).
- [20] P. Puschnig, S. Berkebile, A. J. Fleming, G. Koller, K. Emtsev, T. Seyller, J. D. Riley, C. Ambrosch-Draxl, F. P. Netzer, and M. G. Ramsey, Science 326, 702 (2009).

- [21] B. Stadtmüller, D. Lüftner, M. Willenbockel, E. M. Reinisch, T. Sueyoshi, G. Koller, S. Soubatch, M. G. Ramsey, P. Puschnig, F. S. Tautz, and C. Kumpf, Nat. Commun. 5, 3685 (2014).
- [22] M. Willenbockel, D. Lüftner, B. Stadtmüller, G. Koller, C. Kumpf, P. Puschnig, S. Soubatch, M. G. Ramsey, and F. S. Tautz, Phys. Chem. Chem. Phys. 17, 1530 (2015).
- [23] B. Stadtmüller, J. Seidel, N. Haag, L. Grad, C. Tusche, G. van Straaten, M. Franke, J. Kirschner, C. Kumpf, M. Cinchetti, and M. Aeschlimann, Phys. Rev. Lett. 117, 096805 (2016).
- [24] P. Puschnig, A. D. Boese, M. Willenbockel, M. Meyer, D. Lüftner, E. M. Reinisch, T. Ules, G. Koller, S. Soubatch, M. G. Ramsey, and F. S. Tautz, J. Phys. Chem. Lett. 8, 208 (2017).
- [25] D. Lüftner, M. Milko, S. Huppmann, M. Scholz, N. Ngyuen, M. Wießner, A. Schöll, F. Reinert, and P. Puschnig, J. Electron Spectrosc. Relat. Phenom. 195, 293 (2014).
- [26] K. Schönauer, S. Weiss, V. Feyer, D. Lüftner, B. Stadtmüller, D. Schwarz, T. Sueyoshi, C. Kumpf, P. Puschnig, M. G. Ramsey, F. S. Tautz, and S. Soubatch, Phys. Rev. B 94, 205144 (2016).
- [27] M. Graus, M. Grimm, C. Metzger, M. Dauth, C. Tusche, J. Kirschner, S. Kümmel, A. Schöll, and F. Reinert, Phys. Rev. Lett. 116, 147601 (2016).
- [28] D. Lüftner, T. Ules, E. M. Reinisch, G. Koller, S. Soubatch, F. S. Tautz, M. G. Ramsey, and P. Puschnig, Proc. Natl. Acad. Sci. USA 111, 605 (2014).
- [29] M. Wießner, D. Hauschild, C. Sauer, V. Feyer, A. Schöll, and F. Reinert, Nat. Commun. 5, 4156 (2014).
- [30] S. Weiß, D. Lüftner, T. Ules, E. M. Reinisch, H. Kaser, A. Gottwald, M. Richter, S. Soubatch, G. Koller, M. G. Ramsey, F. S. Tautz, and P. Puschnig, Nat. Commun. 6, 8287 (2015).
- [31] M. P. Seah and W. A. Dench, Surf. Interface Anal. 1, 2 (1979).
- [32] S. Weiß, I. Krieger, T. Heepenstrick, S. Soubatch, M. Sokolowski, and F. S. Tautz, Phys. Rev. B 96, 075414 (2017).
- [33] C. Schneider, C. Wiemann, M. Patt, V. Feyer, L. Plucinski, I. Krug, M. Escher, N. Weber, M. Merkel, O. Renault, and N. Barrett, J. Electron Spectrosc. Relat. Phenom. 185, 330 (2012).
- [34] L. Broekman, A. Tadich, E. Huwald, J. Riley, R. Leckey, T. Seyller, K. Emtsev, and L. Ley, J. Electron Spectrosc. Relat. Phenom. 144-147, 1001 (2005).
- [35] A. Gottwald, R. Klein, R. Müller, M. Richter, F. Scholze, R. Thornagel, and G. Ulm, Metrologia 49, S146 (2012).

- [36] X. Gonze, B. Amadon, P.-M. Anglade, J.-M. Beuken, F. Bottin, P. Boulanger, F. Bruneval, D. Caliste, R. Caracas, M. Côté, T. Deutsch, L. Genovese, Ph. Ghosez, M. Giantomassi, S. Goedecker, D. Hamann, P. Hermet, F. Jollet, G. Jomard, S. Leroux, M. Mancini, S. Mazevet, M. Oliveira, G. Onida, Y. Pouillon, T. Rangel, G.-M. Rignanese, D. Sangalli, R. Shaltaf, M. Torrent, M. Verstraete, G. Zerah, and J. Zwanziger, Comput. Phys. Commun. 180, 2582 (2009), 40 YEARS OF CPC: A celebratory issue focused on quality software for high performance, grid and novel computing architectures.
- [37] G. Kresse and J. Hafner, Phys. Rev. B 47, 558(R) (1993).
- [38] G. Kresse and D. Joubert, Phys. Rev. B 59, 1758 (1999).
- [39] J. P. Perdew, K. Burke, and M. Ernzerhof, Phys. Rev. Lett. 77, 3865 (1996).
- [40] J. Neugebauer and M. Scheffler, Phys. Rev. B 46, 16067 (1992).
- [41] P. E. Blöchl, Phys. Rev. B 50, 17953 (1994).
- [42] H. J. Monkhorst and J. D. Pack, Phys. Rev. B 13, 5188 (1976).
- [43] M. Methfessel and A. T. Paxton, Phys. Rev. B 40, 3616 (1989).
- [44] S. Gärtner, B. Fiedler, O. Bauer, A. Marele, and M. M. Sokolowski, Beilstein J. Org. Chem. 10, 2055 (2014).
- [45] A. Tkatchenko and M. Scheffler, Phys. Rev. Lett. 102, 073005 (2009).

- [46] V. G. Ruiz, W. Liu, E. Zojer, M. Scheffler, and A. Tkatchenko, Phys. Rev. Lett. 108, 146103 (2012).
- [47] O. Bauer, G. Mercurio, M. Willenbockel, W. Reckien, C. H. Schmitz, B. Fiedler, S. Soubatch, T. Bredow, F. S. Tautz, and M. Sokolowski, Phys. Rev. B 86, 235431 (2012).
- [48] I. Adawi, Phys. Rev. 134, A788 (1964).
- [49] P. J. Feibelman and D. E. Eastman, Phys. Rev. B 10, 4932 (1974).
- [50] A. Damascelli, Phys. Scr. **T109**, 61 (2004).
- [51] E. M. Reinisch, T. Ules, P. Puschnig, S. Berkebile, M. Ostler, T. Seyller, M. G. Ramsey, and G. Koller, New J. Phys. 16, 023011 (2014).
- [52] M. Dauth, M. Graus, I. Schelter, M. Wießner, A. Schöll, F. Reinert, and S. Kümmel, Phys. Rev. Lett. 117, 183001 (2016).
- [53] J. W. Gadzuk, Phys. Rev. B 10, 5030 (1974).
- [54] S. Moser, J. Electr. Spectr. Rel. Phenom. 214, 29 (2017).
- [55] A. Schmidt, T. J. Schuerlein, G. E. Collins, and N. R. Armstrong, J. Phys. Chem. 99, 11770 (1995).
- [56] M. Willenbockel, B. Stadtmüller, K. Schönauer, F. Bocquet, D. Lüftner, E. M. Reinisch, T. Ules, G. Koller, C. Kumpf, S. Soubatch, P. Puschnig, M. G. Ramsey, and F. S. Tautz, New J. Phys. 15, 033017 (2013).